Cell Reports

Resource

Modeling the Spatiotemporal Dynamics of Light and Heat Propagation for In Vivo Optogenetics

Graphical Abstract

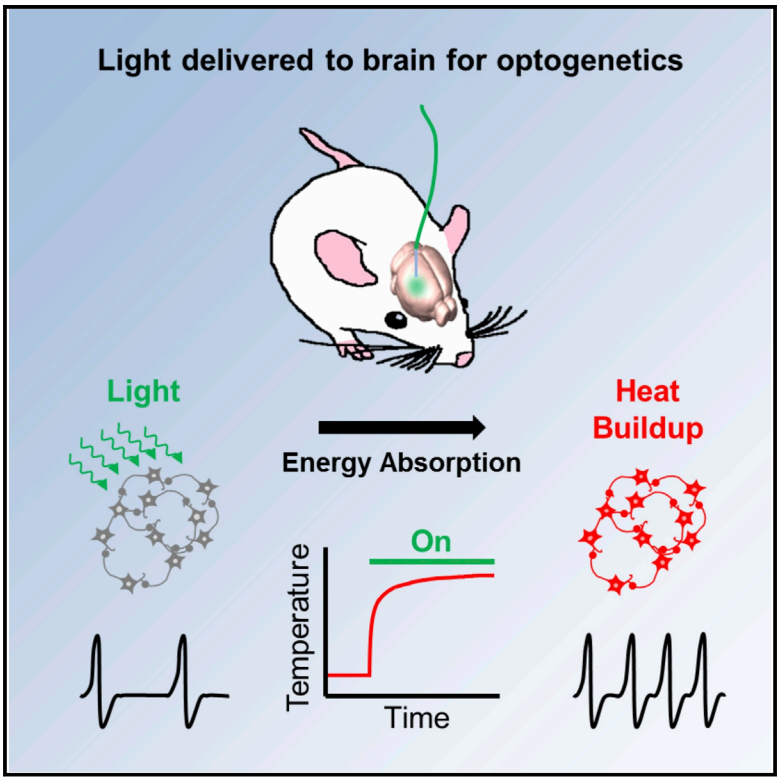

Highlights

- Fiber optic light delivery is sufficient to increase cortical firing rates in vivo
- An optogenetics MATLAB package is provided for predicting light and heat spread
- In vivo temperature recordings validate model predictions of heat induction

Authors

Joseph M. Stujenske, Timothy Spellman, Joshua A. Gordon

Correspondence

jms2317@columbia.edu (J.M.S.), jg343@columbia.edu (J.A.G.)

In Brief

Stujenske et al. demonstrate that light emitted into the brain for optogenetics is sufficient to increase local temperature and the firing rates of single neurons. They provide a software package for modeling light and heat spread from optical fibers.

Stujenske et al., 2015, Cell Reports *12*, 525–534
July 21, 2015
http://dx.doi.org/10.1016/j.celrep.2015.06.036

CellPress

Cell Reports
Resource

Modeling the Spatiotemporal Dynamics of Light and Heat Propagation for In Vivo Optogenetics

Joseph M. Stujenske,[1,*] Timothy Spellman,[2] and Joshua A. Gordon[3,4,*]
[1]Graduate Program in Neurobiology and Behavior, Columbia University, College of Physicians and Surgeons, New York, NY 10032, USA
[2]Feil Family Brain and Mind Research Institute, Weill Cornell Medical College, New York, NY 10021, USA
[3]Department of Psychiatry, Columbia University, College of Physicians and Surgeons, New York, NY 10032, USA
[4]Division of Integrative Neuroscience, New York State Psychiatric Institute, New York, NY 10032, USA
*Correspondence: jms2317@columbia.edu (J.M.S.), jg343@columbia.edu (J.A.G.)
http://dx.doi.org/10.1016/j.celrep.2015.06.036

SUMMARY

Despite the increasing use of optogenetics in vivo, the effects of direct light exposure to brain tissue are understudied. Of particular concern is the potential for heat induced by prolonged optical stimulation. We demonstrate that high-intensity light, delivered through an optical fiber, is capable of elevating firing rate locally, even in the absence of opsin expression. Predicting the severity and spatial extent of any temperature increase during optogenetic stimulation is therefore of considerable importance. Here, we describe a realistic model that simulates light and heat propagation during optogenetic experiments. We validated the model by comparing predicted and measured temperature changes in vivo. We further demonstrate the utility of this model by comparing predictions for various wavelengths of light and fiber sizes, as well as testing methods for reducing heat effects on neural targets in vivo.

INTRODUCTION

Optogenetic tools have proven extremely useful for modulating neural activity in a wide variety of model systems (Boyden et al., 2005; Fenno et al., 2011), allowing for the activation or inactivation of neural activity with unparalleled temporal, anatomical, and cell-type specificity (Williams and Deisseroth, 2013). Optogenetic experiments rely on the expression of exogenous light-activated pumps and channels, which generate depolarizing or hyperpolarizing currents when exposed to light. Typically, light is delivered into the brain through a fiber optic attached to a laser or high-power light-emitting diode (LED) driver. Thus, these experiments often require prolonged illumination of neural tissue with high-intensity light, which may cause biophysically relevant temperature changes (Han, 2012; Acker et al., 2012, Soc. Neurosci., abstract; Christie et al., 2013). Although estimates have been made for calculating induced temperature changes, a biophysically realistic model of light-induced temperature changes in the brain is lacking (Yizhar et al., 2011).

The importance of temperature for neural function has been investigated previously. Raising or lowering bath temperatures leads to changes in resting membrane potential, spontaneous spiking, input resistance, membrane time constant, and synaptic activity in acute slices (Thompson et al., 1985; Kim and Connors, 2012; Volgushev et al., 2000). Evoked synaptic responses also have been reported to vary with temperature in vivo (Andersen and Moser, 1995; Moser et al., 1993). In fact, this effect of temperature has been exploited experimentally to reduce ongoing neural activity by cooling (Long and Fee, 2008; Ponce et al., 2008). Thus, optogenetics introduces the possibility of inducing physiological effects on the basis of heat alone, even in the absence of opsin expression (Han, 2012; Yizhar et al., 2011).

Heat changes induced by optical stimulation have not been extensively tested, but existing data suggest that the temperature change induced by continuous light stimulation can be sufficient to alter both neural and hemodynamic activity (Acker et al., 2012, Soc. Neurosci., abstract; Christie et al., 2013; Desai et al., 2011). We sought to model the spatial and temporal dynamics of heat induced by light stimulation by combining existing models for light and heat spread within three-dimensional tissue (Wang et al., 1995; Pennes, 1948). We tested the results of this model in vivo, finding it to be an accurate predictor of the magnitude and time course of heat induction. This model has been implemented in a MATLAB (MathWorks) package for use by others in designing optogenetic experiments.

RESULTS

Modeling Light Intensity in the Brain

We simulated light spread from an optical fiber with a Monte Carlo simulation of a random walk of photon packets through three-dimensional space (Figure 1A, Monte Carlo). This was contrasted to the way that light is output from a fiber in a non-scattering medium, such as air or water (Figure 1A, Idealized). To realistically simulate light output from an optical fiber, we developed an approach for the initiation of photons into the simulation based on the light acceptance properties of the fiber. Since light can only travel along the length of the fiber at particular angles, we randomized the starting trajectories of photon packets

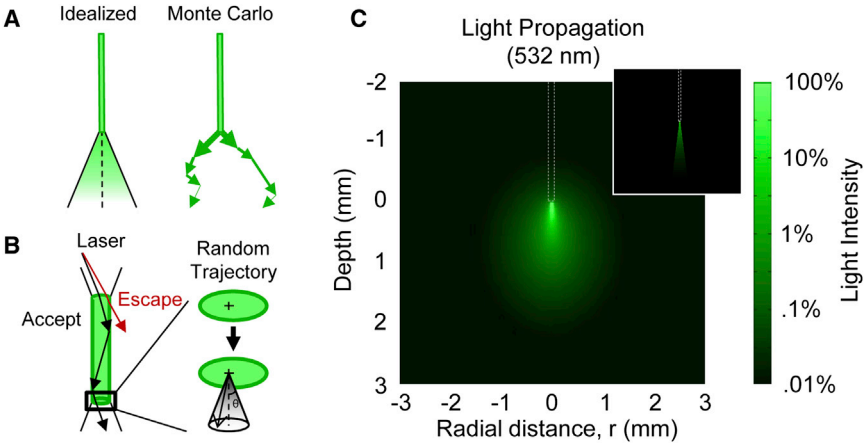

Figure 1. Monte Carlo Simulations Can Predict Light Spread through the Brain in Three Dimensions

(A) Depiction shows the difference between models with idealized light spread (left) and light spread simulating absorption and scattering in media (right).

(B) Model for coupling between a laser emitting collimated light and a fiber optic cable (left) and the method for incorporating this model into photon initiation in the Monte Carlo simulation (right).

(C) Fluence rate (intensity) predicted for 532 nm light out of an optical fiber (62 μm, NA 0.22) by Monte Carlo simulation as a function of distance from the fiber. (Inset) Intensity predicted for an idealized model as in (A).

See also Figure S1.

such that they could not exceed the acceptance angle relative to the normal of the circular fiber end (Figure 1B; Equation 2). Light spread and scatter within the tissue was then simulated using a model previously published by Wang, Jacques, and Zheng (Wang et al., 1995; Jacques, 2011), which treats photons as belonging to discrete packets with an initial energy. Energy from these photon packets is absorbed as they move stochastically through the tissue, leading to both light attenuation and heat buildup.

We have implemented this Monte Carlo simulation as a MATLAB function, MonteCarloLight (Folder S1, Software S1), using scattering and absorption coefficients interpolated from published values, calculated from in vivo data (Johansson, 2010). Using this tool, we generated a predicted propagation pattern for 532 nm light emitting out a 62 μm (numerical aperture [NA] 0.22) optical fiber (Figure 1C; generated with function LightHeatPlotter, Folder S1, Software S5). The light intensity spread predicted by the Monte Carlo simulation is notably wider than that predicted by the idealized model (Figure 1C); the Monte Carlo simulation also predicts increased light intensity dorsal to the fiber tip due to back-scattering. Our results correspond well with a previously published Monte Carlo simulation (Bernstein et al., 2008). Consistent with previous studies, light intensity below the fiber cannot merely be approximated by an exponential fit (Aravanis et al., 2007), regardless of fiber optic size (Figure S1).

Modeling Heat Diffusion in the Brain

The possibility for heat buildup around the tip of the fiber is a potential experimental concern, as even small fluctuations in temperature can have measurable effects on neuronal function (Kim and Connors, 2012; Wang et al., 2011). For this reason, we sought to expand our light transport model to simulate heat changes in neural tissue during illumination with either continuous or pulsed light.

It is reasonable to assume that heat propagation through the tissue can be ignored for short pulses of light and that temperature changes can be predicted by treating light absorption as linear with pulse duration (Yizhar et al., 2011; Aravanis et al., 2007). These methods predict large temperature changes, even for stimulation epochs on the order of 50 ms. To improve on these efforts, we modified Pennes's bio-heat equation (Pennes, 1948) to develop a biophysically realistic model that predicts heat changes, taking into account incident light energy as well as additional variables that affect temperature in the brain, namely, perfusion by blood vessels, metabolic heat production, and heat diffusion in three-dimensional space (Equation 9). This heat diffusion model was implemented as a MATLAB function, HeatDiffusionLight (Folder S1, Software S2).

To investigate the usefulness of our model for predicting temperature changes induced by illumination through a fiber optic, we simulated the temperature change for continuous 10 mW output of 532 nm from a fiber optic (Figure 2A; 62 μm, 0.22 NA). The model predicted a steady buildup of temperature below the fiber over 60 s of illumination (Figure 2B), with a plateau at an average increase of ~2.2°C for depths within a few hundred microns of the fiber tip (temperatures at different depths were calculated as the average in successive circular slices with radius of 250 μm). The maximum temperature increase achieved in a single voxel was 4.1°C (Figure S2A). Steady state was taken to be the temperature after 60 s of illumination, though a small amount (<5%) of additional temperature increase was observed from 60 to 120 s. At steady state, increases of 1°C or greater were observed within roughly a 1 mm^3 cubic volume, despite the fact that light intensities were strongly concentrated only within a few hundred microns of the fiber tip (Figure S2A).

Adding the step of modeling heat diffusion in the brain puts the disparity between light and heat spread in stark relief (Figures 3A and 3B; Figure S2A). To our surprise, we found that first-order approximations of temperature change, ignoring heat diffusion, dramatically overestimated temperature changes even when light pulse durations were very short (Figure 2C, inset). Of course, for long light durations, the two models dramatically diverged (Figure 2C; Figure S2B). Importantly, temperature changes even could be observed above the fiber tip and increased linearly with power (Figure S3). We also evaluated the impact of heat convection on the results of our simulations; while removal of the heat convection term (and also the metabolic heat term to maintain equilibrium) had little effect on the initial phase of heating, it led to a slight elevation of the steady-state temperature (Figure S4). Thus, convection is a less important factor than conduction in the dissipation of heat induced by optogenetic stimulation.

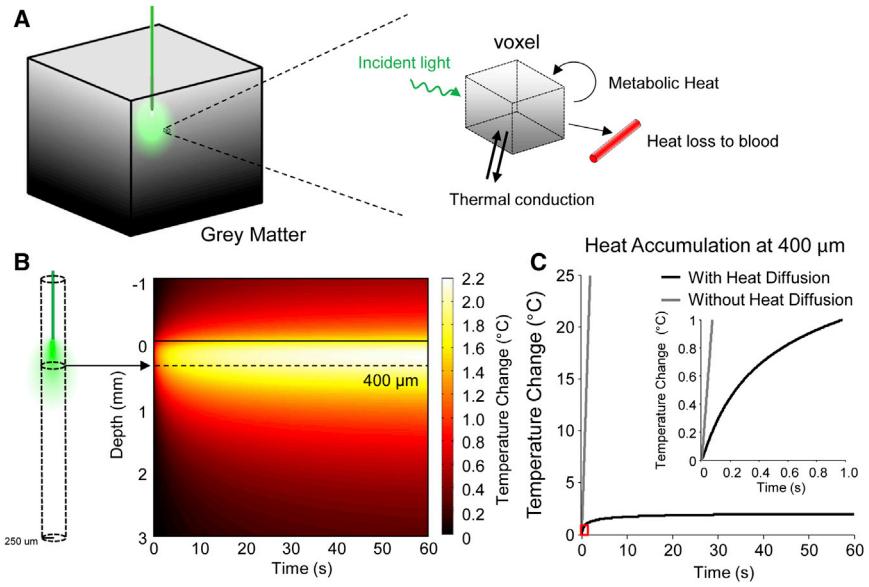

Figure 2. Realistic Bio-Heat Models Can Predict Light-Induced Temperature Change

(A) Depiction shows the combination of Monte Carlo simulation with the Pennes bio-heat equation for modeling light-induced heat changes in a homogenous block of brain.

(B) Heat changes predicted by the bio-heat model for 532 nm light from an optical fiber (62 μm, NA 0.22), plotted as a function of time and depth. Heat was calculated as the average heat change in circles of 250 μm radius, concentric with optical fibers.

(C) Temperature change for the bio-heat model with (black) and without (gray) heat diffusion as a function of time at the depth of 400 μm, as marked by the stippled line in (B).

See also Figures S2–S4.

Overall, our simulations indicate that adding in a biophysically realistic model of heat diffusion leads to a potentially more realistic, and more widespread, estimation of temperature increases in the brain and that incorporation of heat diffusion is necessary for accurate temperature predictions, even for very short light pulses.

Validating Model Parameters

To test the accuracy of our simulations and to select the appropriate parameters for light scattering and absorption from among those in the literature, we compared our predictions to temperature measurements conducted during fiber optic illumination in the brains of anesthetized mice in vivo. While we chose to use scattering and absorption parameters obtained in vivo (Figures 3A and 3B, Parameters 1; Experimental Procedures; Johansson, 2010), a set of parameters obtained in vitro also has been frequently cited in the literature (Figures 3A and 3B, Parameters 2; Experimental Procedures; Yaroslavsky et al., 2002). We first examined the extent to which the differences in parameters affect predicted temperature changes. We compared light propagation and steady-state temperature changes using both parameter sets for simulated 532 nm light (10 mW) emanating from a 62 μm optical fiber (0.22 NA). Both sets of parameters featured similar scattering coefficients, and the predicted light spread was similar between the two models (Figure 3A), with only a ±20% difference in light intensity within 3 mm of the fiber. However, the two sets of parameters differ considerably with respect to their absorption coefficients. Perhaps due to absorption of light by blood, which is largely cleared away in in vitro slices, the absorption coefficient for green light calculated by Johansson (2010) is 5-fold larger than that reported by Yaroslavsky et al. (2002). Accordingly, Parameters 1 predicted a 300%–500% larger temperature increase than Parameters 2 (Figure 3B), demonstrating how temperature prediction depends critically on accurate estimates of the absorption coefficient of brain tissue. Thus, previous studies of light spread (Yizhar et al., 2011; Aravanis et al., 2007; Bernstein et al., 2008) would not be sensitive to the choice of model parameters, while heat predictions would be highly affected.

To test the accuracy of the model with the two parameter sets, we measured heat changes in brain tissue in vivo under continuous light stimulation. Anesthetized mice were implanted with a thermistor and an optical fiber (532 nm wavelength, 10 or 20 mW, 62 μm diameter fiber, 0.22 NA) opposing each other (anti-parallel, with centers aligned), and the distance between the tips of the thermistor and fiber was systematically varied (Figure 3C). The temperature changes we recorded were close to those predicted by the model using the in vivo-derived Parameters 1, though they underestimated temperature changes for short distances by as much as 1°C. This discrepancy was well explained by direct effects of light on the thermistor; high-intensity light heats the thermistor directly, an effect that we measured in a temperature-controlled saline bath. Incorporating this artifact into the model improved correspondence of the data with the simulation (Figure 3C, dashed lines). The temperature changes predicted by the in-vitro-derived Parameters 2 were several-fold smaller, suggesting that they underestimate the temperature change induced by optical illumination in vivo (Figure 3C). It is notable that our predicted temperature distribution peaked at 100–200 μm of depth, while the recorded data did not. Several experimental variables might account for this discrepancy, including non-homogeneity in the tissue (e.g., some small amount of fluid or blood collecting near the fiber tip), increased sensitivity of the thermistor probe at its center (we assumed uniform sensitivity), or experimental error preventing perfect alignment of the fiber with the thermistor.

We also compared our model predictions to previously published peak temperature changes of 0.42°C/mW for blue (445 nm; 200 μm fiber) light stimulation (Christie et al., 2013). Our model slightly underestimated these changes, predicting 0.35°C/mW for 445 nm light, possibly owing to linear

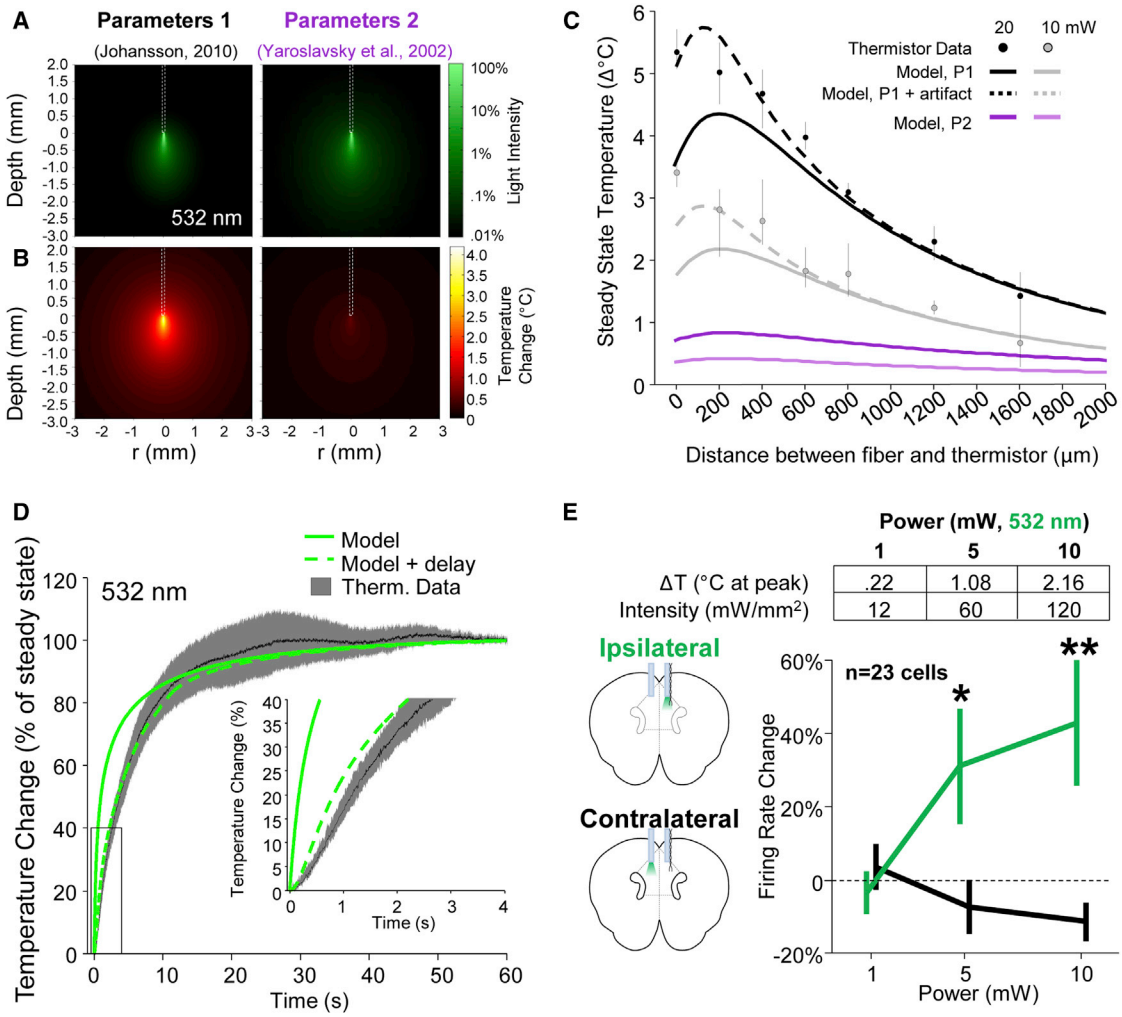

Figure 3. Optical Parameters Measured In Vivo Yield Accurate Predictions of Temperature Change

(A) Fluence rate using optical parameters from Johansson (2010) (left) and Yaroslavsky et al. (2002) (right).

(B) Temperature change for model parameters as in (A).

(C) Temperature changes measured for various distances between an optical fiber (532 nm, 62 μm, NA 0.22) and a thermistor for both 10 (gray circles) and 20 mW (black circles) power output. Error bars indicate the range of all measured temperatures across five repetitions. On the same axes, predicted temperature change as a function of depth is plotted for both sets of model parameters with 10 and 20 mW light power. The effects of direct light also were included and plotted for the first model (dashed lines).

(D) Temperature change as a function of time from light onset for 20 mW light power recorded at a thermistor 400 μm away from an optical fiber. Super-imposed are the predictions for the model with (green, dashed) and without (green) a compensatory delay measured for the thermistor. Error bars indicate the entire range of recorded values.

(E) (Left) Schema for single-unit recordings with an optrode (fiber and stereotrode bundle) in the PFC. During ipsilateral stimulation, light (532 nm through 200 μm, 0.22 NA fiber) was delivered on the same side that the single units were recorded, while during contralateral stimulation, light was delivered on the opposite side. (Right) Predicted peak temperature changes (after 30 s of illumination) and intensity values at the location of the stereotrode bundle (400 μm below the fiber tip) are plotted in the box above for the three light powers tested (1, 5, and 10 mW). Firing rate of single units in the PFC during 30 s periods of light illumination are plotted for these light powers (averaged across five repetitions) for ipsilateral (green) and contralateral (black) illumination. Firing rate was calculated as the percentage change from before illumination. *$p < 0.05$, **$p < 0.01$, Wilcoxon signed-rank test between ipsilateral and contralateral conditions; n = 23 single units from three mice.

extrapolation of the absorption and scattering coefficients for 445 nm from the published values at 480 and 560 nm (Johansson, 2010), which do not capture the large hemoglobin absorption peak between 400 and 450 nm (Booth et al., 2010).

Light-Induced Temperature Quickly Reaches Steady State

A strong advantage to modeling, compared to experimentally measuring temperature change, is the ability to predict the time course of temperature changes. Any device utilized to

measure temperature change will have an intrinsic delay. When we tested the temporal dynamics of our model compared to measurements made with a thermistor, the model reached steady state more rapidly than the thermistor (Figure 3D), as expected. When we compensated for the delay of the thermistor by adding a computationally induced delay to account for the temporal dynamics of the thermistor (see Experimental Procedures), the model still had a slightly faster initial temperature increase, though the time to reach 90% of steady state was similar (Figure 3D). The same delay was found for the offset kinetics (Figure S5A). As expected, there was no significant effect of light power on the temporal dynamics (Figures S5B and S5C). Overall, these data suggest that, at 400 μm below the fiber, 80% of the steady-state temperature change is achieved within 5 s of light onset and 90% of the steady-state temperature is reached by 14 s (Figure 3D; Figures S3B and S3C). Note that, as expected, this is slower than the temporal dynamics previously reported for brain tissue immediately below a fiber optic (Christie et al., 2013). Deeper locations were slower to reach steady state after both light onset and offset.

Temperature Changes from Fiber Optic Illumination Are Sufficient to Induce Firing Rate Changes In Vivo

It has been demonstrated previously that increases in temperature can elevate neuronal firing rate (Reig et al., 2010). We sought to investigate whether the temperature changes induced by fiber optic illumination, as in optogenetic experiments, are sufficient to alter neuronal activity. Wild-type mice, without any opsin expressed, were implanted with optrodes in the prefrontal cortex; each optrode consisted of a 200 μm fiber optic affixed to a stereotrode bundle, with contacts 300–500 μm below the fiber tip. Predicted intensities and temperatures at 400 μm below the fiber were calculated for three light intensities of 532 nm light as follows: 1, 5, and 10 mW (Figure 3E). Illumination and recording were performed during periods of quiet restfulness.

We found that the commonly used intensities of 5 or 10 mW of light illumination were sufficient to elicit increases in firing rates of 31.3% ± 16.2% and 42.9% ± 17.4%, respectively (Figure 3E), while 1 mW was not (−4.9% ± 6.0% change). These illumination intensities corresponded to >1°C change in temperature. With respect to absolute firing rate, at 10 mW, this change corresponded to a modest but significant increase of 0.63 ± 0.21 Hz ($p < 0.01$, paired t test; baseline firing: 4.9 ± 1.0 Hz). To control for other potential confounds of fiber optic illumination (e.g., potential visually evoked responses), we recorded activity when light was delivered through a fiber contralateral to the recording electrode; no significant effect of contralateral illumination on firing rate was seen (Figure 3E; $p > 0.05$). Overall, these data suggest that, consistent with data from acute brain slices, small changes in temperature induced by fiber optic illumination are sufficient to elicit increases in firing rate. It is notable that this effect on firing rate was not seen in the same mice when they were engaged in a prefrontal-dependent spatial working memory task (Spellman et al., 2015), suggesting that temperature-induced effects on firing rate can be state dependent.

Predicting Heat Changes for Different Experimental Protocols

The simulations and experiments described above demonstrate that fiber optic illumination can cause physiologically significant elevations in temperature of the brain. We next evaluated how variations in experimental design, including light wavelength, fiber diameter, and dynamics of light delivery, differentially affected light and heat spread.

Typically, the wavelength is chosen based on the peak sensitivity of the opsin, which varies considerably (and often by design). Inhibitory opsins, in particular, range from peak absorption in the green (Archaerhodopsin) to yellow (Halorhodopsin) and even red (Halo57) spectrum. We modeled light propagation of the most commonly used wavelengths, as illustrated in Figure 4. Iso-contour lines are illustrated for 3 and 10 mW/mm^2 light intensities (Figure 4A), which are in the range of the effective power density for 50% activation (EPD50) for various opsins (Mattis et al., 2012). Our results for blue (473 nm) light correspond well with the extent of c-*fos* activation previously shown for ChR2-expressing cells (Root et al., 2014). Not surprisingly, longer wavelength light penetrated deeper and spread more laterally than shorter wavelength light, owing to slightly lower scattering by the tissue (as noted above, absorption coefficient is not a significant factor in the attenuation of light intensity). Likewise, higher wavelengths were associated with smaller temperature changes since they are less readily absorbed by tissue (Figure 5). There was nearly double the temperature increase for 532 nm light as for 593 nm light, suggesting that experiments optimized for Halorhodopsin may be less susceptible to temperature-induced artifacts than those optimized for Archaerhodopsin.

We also evaluated the effect of fiber size on light spread and heat induction, as fiber sizes varying between 5 (Royer et al., 2010) and 300 μm in diameter (Goshen et al., 2011) have been used for optogenetic manipulations in vivo. We simulated light and heat spread using two commonly used fiber diameters, 62 and 200 μm. Unexpectedly, the fiber diameter had remarkably little bearing on the brain volume achieving light intensities necessary for opsin activation. While there were differences in intensity close to the fiber surface (Figure S6), both fibers seem to be equally suited for large-volume illumination for the purpose of optogenetic manipulation when using high-intensity light (>1 mW; Figure S6). By contrast, the higher light intensity at the tip of a smaller fiber optic, in excess of what is required for opsin activation, translated into a higher predicted heat buildup locally. Indeed, we found that temperature increases within a few hundred microns of the fiber tip were much larger for a 62 μm fiber compared to a 200 μm fiber (Figure 4A). This corresponded to over a 50% increase in peak temperature (largest temperature increase in a single voxel; Figure 4B). Temperature changes at locations farther away from the tip were similar between the two fiber types (Figure 4C). These experiments suggest that larger fiber diameters may reduce the likelihood of temperature-based artifacts without substantial differences in illuminated volume.

The dynamics of light delivery might also affect temperature changes. A recent study by Znamenskiy and Zador used pulsed green light for the inhibition of cells expressing Archaerhodopsin-3 (Znamenskiy and Zador, 2013). Light was presented as 1 ms pulses of 50 mW light every 10 ms (duty cycle of 10%),

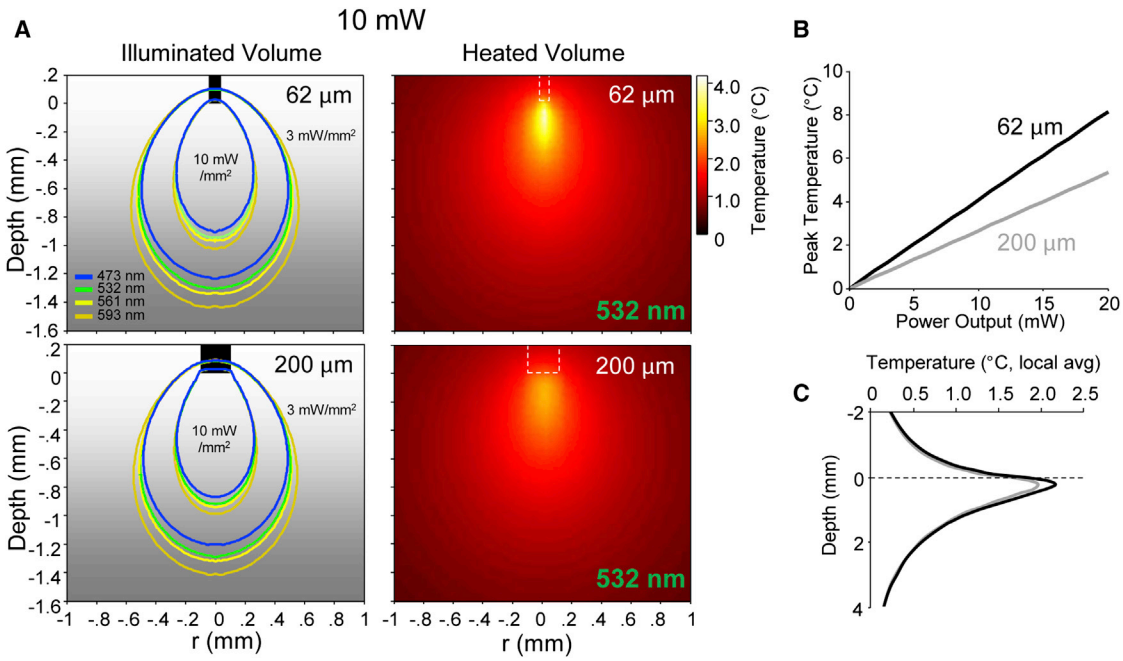

Figure 4. The Effect of Fiber Size on Light Propagation and Heat Induction

(A) (Left) Iso-contour lines for light intensity predicted by the Monte Carlo simulation as a function of distance from the fiber (0.22 NA) for 10 mW of various wavelengths of light out of a 62 (top) and 200 µm (bottom) fiber. (Right) Predicted temperature changes for 10 mW, 532 nm light for a 62 (top) and 200 µm (bottom) fiber.

(B) Peak temperature change (maximum temperature change in a voxel) as a function of power output for 62 and 200 µm fibers, as in Figure 3D.

(C) Temperature change as a function of depth, quantified as in (A) for the 62 and 200 µm fiber of Figure 3D.

See also Figures S5 and S6.

which was predicted to correspond to an effective 5 mW power. To test whether this is an effective strategy for reducing heat while maintaining high light-intensity levels, we simulated pulsing 10 mW of 473 nm light (62 µm fiber) at a 50% and 10% duty cycle and compared it to continuous light (100% duty cycle; Figure 6). As expected, temperature changes oscillated with the duty cycle, but the heat buildup was otherwise equivalent to continuous light at a reduced power, proportional to the duty cycle (e.g., 5 for 10 mW at 50% duty cycle). We used a cycle duration of 100 ms, but we found that shorter or longer cycle durations yielded the same results. Thus, pulsing light is an effective strategy for reducing induced heat while still achieving the volumetric coverage of high light intensities, and it should be considered if light-induced effects are observed in opsin-negative control animals.

DISCUSSION

In this study, we evaluated a model of light and heat spread that simulated the effects of fiber optic illumination of the brain on tissue temperature. We also validated a set of parameters, which, in combination with our model, accurately predicted the extent and timing of heat changes induced in mouse brain tissue by illumination through an optical fiber. We further demonstrated that these modest temperature changes are sufficient to alter neural activity in vivo. We have reported several useful applications of this modeling method, including predicting heat changes for various power outputs, wavelengths, and optical fiber sizes, and we confirmed light pulses as a viable means for reducing induced temperature changes. Finally, we provide a MATLAB toolbox that instantiates the model for use in the design of optogenetic experiments by the neuroscience community.

While we believe that the results of our modeling are informative for understanding the way that light and heat spread during optogenetic experiments, it is important to note that the results of this modeling assume illumination in homogenous gray matter with equal vascularization. In practice, variations in gray and white matter and vascularization will affect the spread of light and heat, and, thus, assumptions of the model will be violated to various extents under different experimental conditions. Nevertheless, our results elucidate several important and generalizable principles of light and heat propagation that are true in all brain tissues.

Illuminating a Desired Brain Volume

For some optogenetic experiments, it is desirable for light illumination to be restricted to a small volume. The model is a simple way to estimate the spread and penetration of light, as well as to test the effect of NA, fiber size, and wavelength on the illuminated volume. A surprising conclusion of the Monte Carlo model utilized here is that light can spread slightly above the end of the fiber tip (Figure 1C), underscoring the usefulness of a realistic model for light propagation in the brain. While region specificity

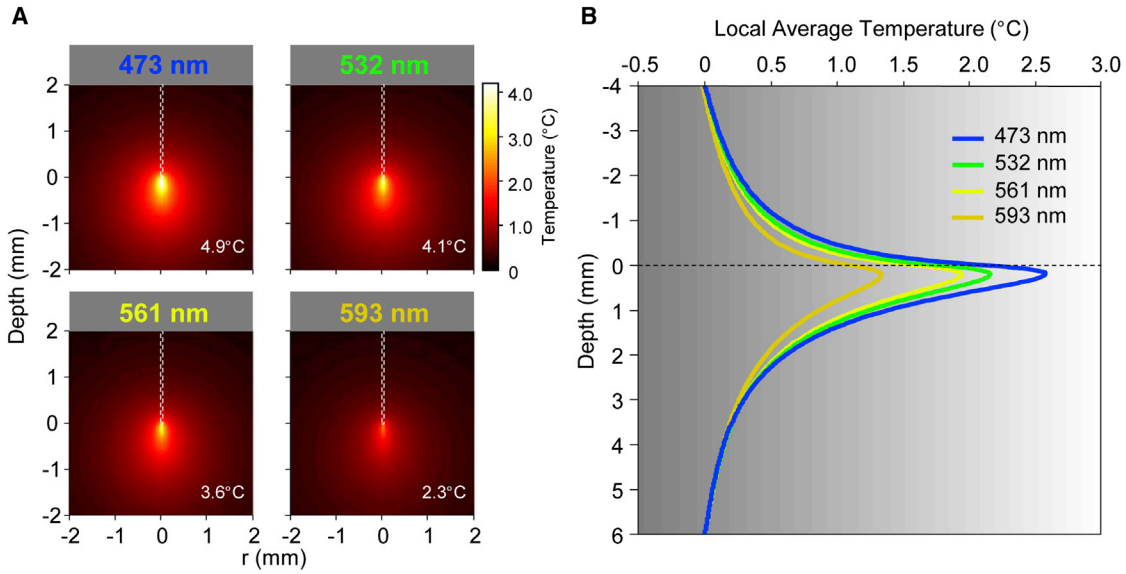

Figure 5. The Effect of Wavelength on Light Propagation and Heat Induction

(A) Predicted temperature change as a function of distance from the optical fiber (62 μm, 0.22 NA) for 473, 532, 561, and 593 nm light. All plots have the same color scale. Text indicates peak temperature in a single voxel.

(B) Predicted temperature change as a function of depth as in (A) for the same wavelengths as in (A).

can often be achieved by limited viral expression, the light itself must be restricted for some applications. For instance, Tye et al. sought to illuminate the terminals of the basolateral amygdala (BLA) in the central amygdala without directly illuminating BLA cells (Tye et al., 2011). To this end, they restricted the light output with a beveled guide cannula, which blocked light out of one side of the fiber. Our model can be helpful for testing the efficacy of interventions of this sort, and, to this end, we have included other functions, MonteCarloLightCartesian and HeatDiffusionLightCartesian (Folder S1, Software S3 and S4), for modeling light scatter that is not symmetric about the central axis.

Controlling for Heat in Optogenetic Experiments

Our work argues for the need of opsin-negative control animals in all optogenetic experiments. In this work, we predict temperature changes for continuous 10 mW light ranging from 1°C to 4°C across a large volume of tissue, depending on wavelength and fiber size. This temperature range is sufficient to induce both physiological and behavioral changes (Thompson et al., 1985; Moser et al., 1993). It is important to note that there can be a dissociation between physiology and behavior as changes in temperature can induce physiological changes in the absence of changes in behavior (Moser and Andersen, 1994). For this reason, physiological as well as behavioral effects from light stimulation should be compared to opsin-negative controls whenever possible, even in the absence of a behavioral change. It is also important to note that the effects of temperature could lead to light-induced effects in non-opsin-expressing cells, thereby compromising the specificity of effects in experiments with cell-type-specific expression.

If effects of light presentation are seen in control animals, one may want to alter the stimulation parameters to reduce confounding effects of heat. To this end, we have provided evidence for the efficacy of pulsing light for reducing heat. Our model also highlights the importance of fiber size on induced heat effects. While light propagation and heat induction are not grossly affected by different fiber sizes, there is a substantial difference in heat induced near the tip of the optical fiber. Larger fiber sizes reduce the temperature around the fiber tip (where the largest heat change occurs), and, thus, they may be favored over smaller tips for certain applications. Lastly, heat-induced effects may be reduced by using opsins activated by higher wavelengths of light, as temperature near the tip is predicted to be approximately 2-fold less when illuminating with 593 nm light compared to 532 nm light.

Indeed, many optogenetic studies have thus far kept temperature changes to a minimum. For instance, several studies have used 5 (Tye et al., 2011; Kim et al., 2013) or 10 mW (Warden et al., 2012) of 593 nm light out of a 200 μm fiber for Halorhodopsin stimulation, predicted by the model to keep temperature increases below 1°C. In these same studies, 5 or 10 mW of 473 nm light (200 μm fiber) were used for activation, which would be predicted to yield a higher temperature change; but, because the light was pulsed with at most a 50% duty cycle, peak temperature increases should have been confined to a range of 0.5°C–0.9°C. Nevertheless, with the increasing use of continuous stimulation with 532 nm light to support Archaerhodopsin-mediated inhibition, heat may become more of a concern as a confounding effect of light stimulation independent of opsin activation.

Concluding Remarks

We provide here, for use by the scientific community, a MATLAB toolbox for modeling light and heat propagation in the brain. We believe this will help researchers to optimally plan experiments,

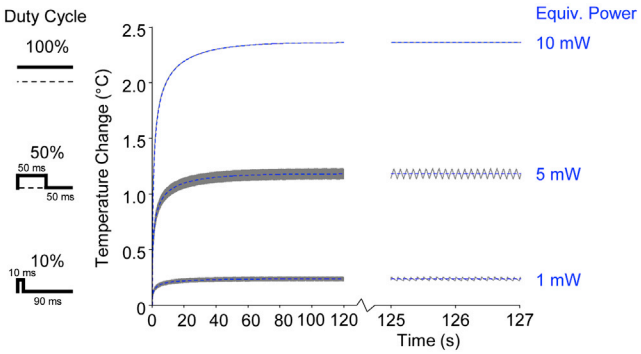

Figure 6. Light-Induced Temperature Change Drops Linearly with Duty Cycle

Predicted temperature change is plotted in gray as a function of time for 10 mW power light out of an optical fiber (473 nm, 62 μm, 0.22 NA) at duty cycles of 100% (top), 50% (middle), and 10% (bottom). Superimposed blue lines indicate predicted temperature changes for continuous 10 (top), 5 (middle), and 1 mW (bottom) light power.

potentially reducing the number of animals used by avoiding experimental pitfalls.

EXPERIMENTAL PROCEDURES

Monte Carlo Modeling of Light Transport

To simulate light propagation in neural tissue, we modeled neural tissue in cylindrical coordinates as a cylinder of 6 mm radius and 10 mm thickness with absorbing ends. Cylindrical voxels were generated, discretizing space in 10 μm steps. Identical results were obtained for a 6 × 6 × 10 mm cube of tissue in Cartesian coordinates using 10 μm^3 voxels, but cylindrical coordinates were favored for computational efficiency. Cylindrical coordinates, however, have the notable problem of increased noise for positions directly below the light source, so care must be taken to run a sufficiently large simulation (10^7 packets of photons were used for all simulations reported, but similar results could be obtained with 10^6 packets). Results were also not sensitive to the size of voxels that were selected, in the range of 5 to 30 μm^3. Light transport through the brain was implemented using an anisotropic scattering model utilizing the Henyey-Greenstein phase function as follows:

$$p(\cos\theta) = \frac{1-g^2}{2(1+g^2-2g\cos\theta)^{3/2}}, \quad \text{(Equation 1)}$$

where g is the anisotropy parameter, between 0 (no anisotropy) and 1 (pure forward scatter).

Photon packets were launched from the tip of an optical fiber located 4 mm deep along the central axis of the tissue. For each packet, the initial starting position was randomized so that it was equally likely to be at any position on the circular surface of the fiber. The initial direction of each packet was then determined from the angle in the plane of the surface, θ, chosen randomly between 0 and 2π, and the angle relative to the orthogonal, φ, which was selected from a random uniform distribution between $\pm\,\theta_{accept}$ given by

$$\theta_{accept} = \sin^{-1}\left(\frac{NA}{n}\right), \quad \text{(Equation 2)}$$

where NA is the numerical aperture (NA = 0.22 for all simulations in this paper) and n is the index of refraction (n = 1.36) of brain (Binding et al., 2011; Aravanis et al., 2007). This models the conical spread of light out of the optical fiber.

Light transport was based on a previously published model (Wang et al., 1995; Jacques, 2011). In brief, the light transport model was initiated with packets of light with weight set to 1. Upon each iteration of the light transport model, light packets were moved a random distance, such that, at time t, the n^{th} light packet moved a distance given by

$$S_{n,t} = \frac{-\log X_n}{\sigma_a + \sigma_s}, \quad \text{(Equation 3)}$$

where σ_a and σ_s are the absorption and scattering coefficients of brain tissue and X_n is a pseudo-random variable uniformly distributed between 0 and 1.

After moving, some of the packet's energy was absorbed by the tissue (and thereby attenuated). This was modeled by dropping the weights of the packets by a factor of $(\sigma_s/\sigma_a + \sigma_s)$ so that

$$w_{n,t+1} = w_{n,t}\frac{\sigma_s}{\sigma_a + \sigma_s}, \quad \text{(Equation 4)}$$

where $w_{n,t}$ is the weight of the n^{th} photon packet at time t, and

$$w^*_{r,z,t+1} = w^*_{r,z,t} + w_{n,t}\frac{\sigma_a}{\sigma_a + \sigma_s}, \quad \text{(Equation 5)}$$

where $w^*_{r,z,t}$ is the total stored weight in the voxel at which the photon packet is located up until time t.

The light is then scattered, choosing a deflection-scattering angle in the radial plane as governed by the Henyey-Greenstein phase function (Equation 1), and the azimuthal-scattering angle in the depth plane is calculated as

$$\varphi_{n,t} = 2\pi Y_n, \quad \text{(Equation 6)}$$

where Y_n is a pseudo-random variable uniformly distributed between 0 and 1.

Photon packets of low weight ($w < 1 \times 10^{-4}$) are extinguished with 90% probability. If not extinguished, their weight is increased by 10-fold with 10% chance. This process allows the model to reach an endpoint without leaking net weights out of the system (conservation of energy). Photon packets that left the simulated tissue were eliminated, but this was a negligible amount of photon energy for the dimensions used. Light that back-scattered upward was allowed to penetrate through the optical fiber as if it were brain tissue for computational simplicity. More complicated models allowing for reflections off the optical fiber were simulated but gave nearly identical results.

After simulation was complete, the fluence rate, the sum total of incident light power from all directions per unit volume at each voxel, $\phi_{r,z}$, was given by

$$\phi_{r,z} = P\frac{w^*_{r,x}}{\mu_a n_{photons} 2\pi(r-0.5)dr^2\,dz}, \quad \text{(Equation 7)}$$

where P is the light power, $n_{photons}$ is the number of photon packets launched in total, dr is the discretization parameter in the radial dimension, and dz is the discretization parameter in the depth dimension. Throughout the paper, light intensity means the fluence rate (mW/mm^2).

Values for σ_s, σ_a, and g were linearly interpolated from in vivo data (Johansson, 2010). Note that the absorption coefficient used is several-fold larger than that reported for in vitro tissue (Yaroslavsky et al., 2002), likely due to the absorption of light by blood and melanin in vivo. Some in vitro measurements have yielded values closer to those obtained in vivo, possibly due to differences in tissue preparation (Gebhart et al., 2006). We directly compared the results obtained by linearly interpolating from in vitro and in vivo data in Figure 3.

Modeling Heat Diffusion

For modeling heat diffusion, tissue was again modeled as a cylinder of 6 mm radius and 10 mm thickness with absorbing boundaries. Heat transport in the brain was treated as a diffusion process using the well-known modification of the diffusion equation, Pennes's bio-heat transfer equation (Pennes, 1948), which has been applied to brain tissue previously (Aronov and Fee, 2011):

$$\rho c\frac{\partial T}{\partial t} = \nabla k\nabla T + \rho_b c_b w_b(T_A - T) + q_m. \quad \text{(Equation 8)}$$

T is the local tissue temperature (37°C at baseline in the absence of heat input); T_A is the temperature of the blood in the main arteries supplying the scalp,

assumed to be constant (36.7°C); and k, ρ, and c are the thermal conductivity, density, and specific heat of the brain, respectively. Values for blood are given by ρ_b and c_b; w_b and q_m are the blood perfusion rate and the metabolic heat production in the tissue, respectively. Variables and input parameters were defined as in Table S1 based on previous studies (Elwassif et al., 2006; Janssen et al., 2005). Equation 9 was modified to incorporate incident light so that

$$\rho c \frac{\partial T}{\partial t} = \nabla k \nabla T + \rho_b c_b w_b (T_A - T) + q_m + \phi\, \mu_a, \qquad \text{(Equation 9)}$$

where ϕ is fluence rate (intensity).

Equation 9 was discretized using a forward difference scheme. Space was discretized using steps, Δx, of 30 μm, which gave very similar results to 10 μm. The optical fiber was treated as equivalent to brain tissue for heat diffusion, for simplicity. To assure numerical stability, time was discretized with steps given by

$$\Delta t = \frac{(\Delta x)^2 \rho c}{6k} = 1.1 \text{ ms}. \qquad \text{(Equation 10)}$$

Animal Use

All animal procedures were conducted in accordance with NIH regulations and approved by Columbia University and New York State Psychiatric Institute Institutional Animal Care and Use Committees.

In Vivo Temperature Measurement

Two mice (male C57/B6, 8–12 weeks old) were deeply anesthetized with isoflurane and mounted into a stereotax. The internal temperature of the mice (measured intra-rectally) was maintained at 36.7 degrees using a heating pad throughout the experiment. A craniotomy was made over the lateral surface of the frontal cortex, on either side. A small, 62 μm diameter optical fiber was coupled to a 532 nm laser (OEM Laser) and passed through the brain from left to right hemisphere. A thermistor probe (Wavelength Electronics, TCS10K5) was pressed firmly into the cortex, anti-parallel to the optical fiber so that their centers aligned. Heat measurements were made before, during, and after 60 s of illumination at various distances between the thermistor and fiber (0–1.6 mm). Both 10 and 20 mW intensities were tested. After surgery, the mice were euthanized with a lethal dose of ketamine.

We chose to use a thermistor because of its high temperature sensitivity at physiological temperatures. Thermistor resistance readings were calibrated to temperature by touching the thermistor tip to temperature-controlled baths of water. As expected, a log-linear relationship was found between resistance and temperature. To compare model outputs to thermistor readings, we accounted for two unavoidable sources of experimental error introduced by the thermistor readings. First, the temporal delays introduced by the thermistor were calculated. In a medium of constant temperature, the temperature reading of the thermistor was found to be accounted for by a simple exponential time constant of about 4 s. However, in our experiment, only part of the metal was in contact with the brain, introducing a non-linearity into the temporal dynamics of the thermistor readings. To correct for this, a temporal kernel was measured by touching the tip of the thermistor to a water bath held at various temperatures (equivalent to step function increase). Since water has a similar thermal conductivity to brain, we reasoned that this should approximately emulate the temporal dynamics in our experiment. The calculated kernel was used to convolve the model output to introduce a non-linear temporal delay. Second, the effects of light directly hitting the thermistor and being absorbed by the metal were modeled. The conversion of incident light power to steady-state resistance changes in the metal were measured in water held at 37°C by illuminating the thermistor with an optical fiber at various distances (0–1.6 mm). There was a measured increase of 2.4×10^{-5}°C/mW/mm^2 at a distance of 0 mm, with the measured temperature change dropping off in a way that was well-modeled by the attenuation of light in saline (non-scattering medium). For modeling, the temporal dynamics for this direct light absorption were treated as having the same non-linear kernel as measured previously.

An important caveat for any means of measuring temperature change is the potential contribution of the device itself to temperature changes in the tissue. In particular, direct heating of the thermistor by incident light might artificially elevate the temperature change in the brain. However, the contribution of direct light absorption was negligible past 1 mm from the fiber, at which distances our model reliably predicted recorded temperature changes in the brain. For this reason, we concluded that incident light on the thermistor did not explain our results.

In Vivo Electrophysiological Recordings

Three mice (male C57/B6, 8–12 weeks old) were placed inside a flow box and anesthetized with isoflurane gas (2%) until sedated, at which point they were placed in a stereotax and maintained on 0.5% isoflurane for the duration of the surgery. Craniotomies were made bilaterally above the prefrontal cortex (mPFC), and skull screws placed over cerebellum and olfactory bulb served as ground and reference, respectively.

An optrode was implanted in the left mPFC (1.8 mm anterior, 0.4 mm lateral, 1.4 mm ventral), while a ferrule-coupled optical fiber (Thorlabs, 200 μm diameter) was implanted over the right mPFC. The optrode consisted of 13 stereotrodes made from 13 μM-diameter tungsten fine wire (California Fine Wire) glued to a ferrule-bound optical fiber positioned 300–500 μm dorsal to the stereotrode tips, which were arrayed semi-circularly around the lateral edge of the fiber.

Recordings were amplified, band-pass filtered (600–6,000 Hz), and digitized using the Neuralynx Digital Lynx system. Spikes were detected by online thresholding and collected at 32 kHz. Units were initially clustered using Klustakwik (Ken Harris, University College London) and sorted according to the first two principal components, voltage peak, and energy for each channel. Clusters were then accepted, merged, or eliminated based on visual inspection of feature segregation, waveform distinctiveness and uniformity, stability across recording session, and ISI distribution. Isolation distances were consistently above 15.

Subsequently, electrothermolytic lesions were made to histologically confirm recording sites. Fiber optic tracks were also visualized.

SUPPLEMENTAL INFORMATION

Supplemental Information includes six figures, one table, and five software files and can be found with this article online at http://dx.doi.org/10.1016/j.celrep.2015.06.036.

AUTHOR CONTRIBUTIONS

J.M.S. and T.S. designed and performed the research. J.M.S. and J.A.G. wrote the paper.

ACKNOWLEDGMENTS

We thank S. Siegelbaum and P. Spitalnik for feedback on the manuscript. This work was supported by grants from the National Institute of Mental Health (NIMH R01 MH081968 and R01 MH096274), the Hope for Depression Research Foundation, and the International Mental Health Research Organization to J.A.G. J.M.S. is supported through the Columbia University Medical Scientist Training Program.

Received: January 13, 2015
Revised: May 13, 2015
Accepted: June 8, 2015
Published: July 9, 2015

REFERENCES

Andersen, P., and Moser, E.I. (1995). Brain temperature and hippocampal function. Hippocampus *5*, 491–498.

Aravanis, A.M., Wang, L.P., Zhang, F., Meltzer, L.A., Mogri, M.Z., Schneider, M.B., and Deisseroth, K. (2007). An optical neural interface: in vivo control of rodent motor cortex with integrated fiberoptic and optogenetic technology. J. Neural Eng. *4*, S143–S156.

Aronov, D., and Fee, M.S. (2011). Analyzing the dynamics of brain circuits with temperature: design and implementation of a miniature thermoelectric device. J. Neurosci. Methods *197*, 32–47.

Bernstein, J.G., Han, X., Henninger, M.A., Ko, E.Y., Qian, X., Franzesi, G.T., McConnell, J.P., Stern, P., Desimone, R., and Boyden, E.S. (2008). Prosthetic systems for therapeutic optical activation and silencing of genetically-targeted neurons. Proc SPIE Int Soc Opt Eng *6854*, 68540H.

Binding, J., Ben Arous, J., Léger, J.-F., Gigan, S., Boccara, C., and Bourdieu, L. (2011). Brain refractive index measured in vivo with high-NA defocus-corrected full-field OCT and consequences for two-photon microscopy. Opt. Express *19*, 4833–4847.

Booth, E., Dukatz, C., Ausman, J., and Wider, M. (2010). Cerebral and somatic venous oximetry in adults and infants. Surg. Neurol. Int. *1*, 75.

Boyden, E.S., Zhang, F., Bamberg, E., Nagel, G., and Deisseroth, K. (2005). Millisecond-timescale, genetically targeted optical control of neural activity. Nat. Neurosci. *8*, 1263–1268.

Christie, I.N., Wells, J.A., Southern, P., Marina, N., Kasparov, S., Gourine, A.V., and Lythgoe, M.F. (2013). fMRI response to blue light delivery in the naïve brain: implications for combined optogenetic fMRI studies. Neuroimage *66*, 634–641.

Desai, M., Kahn, I., Knoblich, U., Bernstein, J., Atallah, H., Yang, A., Kopell, N., Buckner, R.L., Graybiel, A.M., Moore, C.I., and Boyden, E.S. (2011). Mapping brain networks in awake mice using combined optical neural control and fMRI. J. Neurophysiol. *105*, 1393–1405.

Elwassif, M.M., Kong, Q., Vazquez, M., and Bikson, M. (2006). Bio-heat transfer model of deep brain stimulation induced temperature changes. Conf. Proc. IEEE Eng. Med. Biol. Soc. *1*, 3580–3583.

Fenno, L., Yizhar, O., and Deisseroth, K. (2011). The development and application of optogenetics. Annu. Rev. Neurosci. *34*, 389–412.

Gebhart, S.C., Lin, W.C., and Mahadevan-Jansen, A. (2006). In vitro determination of normal and neoplastic human brain tissue optical properties using inverse adding-doubling. Phys. Med. Biol. *51*, 2011–2027.

Goshen, I., Brodsky, M., Prakash, R., Wallace, J., Gradinaru, V., Ramakrishnan, C., and Deisseroth, K. (2011). Dynamics of retrieval strategies for remote memories. Cell *147*, 678–689.

Han, X. (2012). Optogenetics in the nonhuman primate. Prog. Brain Res. *196*, 215–233.

Jacques, S. (2011). Monte Carlo modeling of light transport in tissue (steady state and time of flight). In Optical-Thermal Response of Laser-Irradiated Tissue, A.J. Welch and M.J.C. Gemert, eds. (Springer Netherlands).

Janssen, F.E., Van Leeuwen, G.M., and Van Steenhoven, A.A. (2005). Modelling of temperature and perfusion during scalp cooling. Phys. Med. Biol. *50*, 4065–4073.

Johansson, J.D. (2010). Spectroscopic method for determination of the absorption coefficient in brain tissue. J. Biomed. Opt. *15*, 057005, 057005–057009.

Kim, J.A., and Connors, B.W. (2012). High temperatures alter physiological properties of pyramidal cells and inhibitory interneurons in hippocampus. Front. Cell. Neurosci. *6*, 27.

Kim, S.-Y., Adhikari, A., Lee, S.Y., Marshel, J.H., Kim, C.K., Mallory, C.S., Lo, M., Pak, S., Mattis, J., Lim, B.K., et al. (2013). Diverging neural pathways assemble a behavioural state from separable features in anxiety. Nature *496*, 219–223.

Long, M.A., and Fee, M.S. (2008). Using temperature to analyse temporal dynamics in the songbird motor pathway. Nature *456*, 189–194.

Mattis, J., Tye, K.M., Ferenczi, E.A., Ramakrishnan, C., O'Shea, D.J., Prakash, R., Gunaydin, L.A., Hyun, M., Fenno, L.E., Gradinaru, V., et al. (2012). Principles for applying optogenetic tools derived from direct comparative analysis of microbial opsins. Nat. Methods *9*, 159–172.

Moser, E.I., and Andersen, P. (1994). Conserved spatial learning in cooled rats in spite of slowing of dentate field potentials. J. Neurosci. *14*, 4458–4466.

Moser, E., Mathiesen, I., and Andersen, P. (1993). Association between brain temperature and dentate field potentials in exploring and swimming rats. Science *259*, 1324–1326.

Pennes, H.H. (1948). Analysis of tissue and arterial blood temperatures in the resting human forearm. J. Appl. Physiol. *1*, 93–122.

Ponce, C.R., Lomber, S.G., and Born, R.T. (2008). Integrating motion and depth via parallel pathways. Nat. Neurosci. *11*, 216–223.

Reig, R., Mattia, M., Compte, A., Belmonte, C., and Sanchez-Vives, M.V. (2010). Temperature modulation of slow and fast cortical rhythms. J. Neurophysiol. *103*, 1253–1261.

Root, C.M., Denny, C.A., Hen, R., and Axel, R. (2014). The participation of cortical amygdala in innate, odour-driven behaviour. Nature *515*, 269–273.

Royer, S., Zemelman, B.V., Barbic, M., Losonczy, A., Buzsáki, G., and Magee, J.C. (2010). Multi-array silicon probes with integrated optical fibers: light-assisted perturbation and recording of local neural circuits in the behaving animal. Eur. J. Neurosci. *31*, 2279–2291.

Spellman, T., Rigotti, M., Ahmari, S.E., Fusi, S., Gogos, J.A., and Gordon, J.A. (2015). Hippocampal-prefrontal input supports spatial encoding in working memory. Nature *522*, 309–314.

Thompson, S.M., Masukawa, L.M., and Prince, D.A. (1985). Temperature dependence of intrinsic membrane properties and synaptic potentials in hippocampal CA1 neurons in vitro. J. Neurosci. *5*, 817–824.

Tye, K.M., Prakash, R., Kim, S.Y., Fenno, L.E., Grosenick, L., Zarabi, H., Thompson, K.R., Gradinaru, V., Ramakrishnan, C., and Deisseroth, K. (2011). Amygdala circuitry mediating reversible and bidirectional control of anxiety. Nature *471*, 358–362.

Volgushev, M., Vidyasagar, T.R., Chistiakova, M., and Eysel, U.T. (2000). Synaptic transmission in the neocortex during reversible cooling. Neuroscience *98*, 9–22.

Wang, L., Jacques, S.L., and Zheng, L. (1995). MCML—Monte Carlo modeling of light transport in multi-layered tissues. Comput. Methods Programs Biomed. *47*, 131–146.

Wang, Y.Y., Qin, J., Han, Y., Cai, J., and Xing, G.G. (2011). Hyperthermia induces epileptiform discharges in cultured rat cortical neurons. Brain Res. *1417*, 87–102.

Warden, M.R., Selimbeyoglu, A., Mirzabekov, J.J., Lo, M., Thompson, K.R., Kim, S.Y., Adhikari, A., Tye, K.M., Frank, L.M., and Deisseroth, K. (2012). A prefrontal cortex-brainstem neuronal projection that controls response to behavioural challenge. Nature *492*, 428–432.

Williams, S.C.P., and Deisseroth, K. (2013). Optogenetics. Proc. Natl. Acad. Sci. USA *110*, 16287.

Yaroslavsky, A.N., Schulze, P.C., Yaroslavsky, I.V., Schober, R., Ulrich, F., and Schwarzmaier, H.J. (2002). Optical properties of selected native and coagulated human brain tissues in vitro in the visible and near infrared spectral range. Phys. Med. Biol. *47*, 2059–2073.

Yizhar, O., Fenno, L.E., Davidson, T.J., Mogri, M., and Deisseroth, K. (2011). Optogenetics in neural systems. Neuron *71*, 9–34.

Znamenskiy, P., and Zador, A.M. (2013). Corticostriatal neurons in auditory cortex drive decisions during auditory discrimination. Nature *497*, 482–485.